# Fullerene-Modified Poly(2,6-dimethyl-1,4-phenylene oxide) Gas Separation Membranes: Why Binding Is Better than Dispersing

**Dana M. Sterescu,[†] Dimitrios F. Stamatialis,*[,†] Eduardo Mendes,[‡] Michael Wübbenhorst,[‡,§] and Matthias Wessling[†]**

*Faculty of Science and Technology, Membrane Technology Group, University of Twente, P.O. Box 217, 7500 AE, Enschede, The Netherlands; Polymer Materials and Engineering, Delft University of Technology, 2628 BL, Delft, The Netherlands; and Department of Physics and Astronomy, Katholieke Universiteit Leuven, Celestijnenlaan 200D, B-3001 Leuven, Belgium*

*Received June 12, 2006; Revised Manuscript Received October 19, 2006*

ABSTRACT: This paper describes the preparation, characterization, and the permeation properties of poly(2,6-dimethyl-1,4-phenylene oxide) (PPO) dense polymer films containing fullerenes ($C_{60}$). The $C_{60}$ are either dispersed or covalently bonded to PPO at various concentrations. The gas permeability results are very different between covalently bonded and dispersed PPO−$C_{60}$. The gas permeability of PPO−$C_{60}$ bonded increases up to 80% with increasing fullerene concentration. The gas pair selectivity, however, stays constant. This behavior is probably due to stiffening of the polymer structure and increase of free volume. The gas permeability through the PPO−$C_{60}$ dispersed decreases in comparison to pure PPO. This reduction is due to $C_{60}$ clustering in the polymer. The clusters seem to induce polymer crystallinity, and they are probably aligned along the film plane, creating an extra barrier for gas permeation.

## 1. Introduction

The control of gas permeability and selectivity for polymer membranes separating molecular mixtures of gases has become a subject of intense research in both the industrial and academic fields.[1] Special attention has been concentrated on the relationship between the polymer structure and gas separation properties. Most of the polymers that have been investigated, however, show the general trend that highly permeable polymers possess rather low selectivity. This often referred to as the permeability/selectivity trade-off relationship.[2]

The permeation properties of a polymer depend primarily on the packing density, the polymer chain mobility, and the free volume of the polymer structure, which can be increased by the introduction of bulky substituents. For this, a considerable interest has been shown in supermolecular carbon cages (fullerene, bucky balls, $C_{60}$) containing polymers.[3−7] The hard-sphere properties of $C_{60}$ may inhibit molecular polymer chain packing, possibly resulting in high free volume and improved permeation properties.

Only very few polymers are actually used for the industrial production of gas separation membranes; poly(2,6-dimethyl-1,4-phenylene oxide) (PPO) is one of them.[8] PPO is particularly interesting for the production of nitrogen-enriched air due to its high permeability and acceptable selectivity. It is highly desirable to identify methods to modify PPO chemically in order to increase permeability without compromising selectivity. In our earlier study,[3] we have shown that the coupling of the bulky $C_{60}$ groups to PPO backbone can increase the gas permeability (up to 80%) without compromise to selectivity. In this paper, we study the permeation properties of PPO−$C_{60}$ dispersed, too. A small amount of $C_{60}$ dispersed into PPO seems to cause significant reduction of membrane permeability. A systematic analysis of both PPO−$C_{60}$ bonded and dispersed is performed using differential scanning calorimetry (DSC), wide-angle X-ray scattering (WAXS) measurements, and gas sorption experiments in order to investigate the reasons of the difference in the permeation performance between the bonded and dispersed $C_{60}$.

## 2. Background

**2.1. Transport in Polymers.** The permeation of a gas molecule through a dense membrane is usually governed by a solution−diffusion mechanism. The permeability, *P*, of a polymer is given as the product of diffusivity, *D* (kinetic component), and solubility, *S* (thermodynamic component):

$$P = DS \tag{1}$$

The ideal selectivity of a membrane for component A relative to component B, $\alpha_{A/B}$, is defined as the ratio of their permeabilities,[9,10] which in terms of eq 1 can be rewritten as

$$\alpha_{A/B} = \frac{P_A}{P_B} = \left(\frac{S_A}{S_B}\right)\left(\frac{D_A}{D_B}\right) \tag{2}$$

The first term on the right-hand side is the solubility selectivity, and the second term is the diffusivity selectivity.

Over the past three decades, sorption of gas molecules into glassy polymers has been described and analyzed by the dual-mode sorption model.[11] The fundamental assumption of the dual mode sorption theory is the existence of two distinct populations of gas molecules in a polymer matrix. Rubbery polymers are in a hypothetical thermodynamic equilibrium liquid state, and their gas solubility obeys Henry's law. On the other hand, glassy polymers are typically assumed to be in a nonequilibrium state containing two components: a frozen-in solid state of unrelaxed free volume and a hypothetical liquid state being in equilibrium. The model is used to represent the sorbed amount of gas (*C*) of pure gases in polymers as a function of the pressure (*p*) and is expressed by

[†] University of Twente.
[‡] Delft University of Technology.
[§] Katholieke Universiteit Leuven.
* Corresponding author. E-mail: d.stamatialis@tnw.utwente.nl.

10.1021/ma061300p CCC: $33.50 
Published on Web 12/02/2006

$$C = C_D + C_H = k_D p + \frac{C'_H b p}{1 + bp} \quad (3)$$

where $C_D$ is the gas concentration based on Henry's law sorption, $C_H$ is the gas concentration based on Langmuir sorption, $k_D$ is the Henry's law coefficient, and $b$ and $C'_H$ are the Langmuir hole affinity parameter and the capacity parameter, respectively. The $k_D$ parameter represents the penetrant dissolved in the polymer matrix at equilibrium, and $b$ characterizes the sorption affinity for a particular gas−polymer system. These parameters can be determined from the measured sorption data. $C'_H$ is often used to measure the amount of the nonequilibrium excess free volume in the glassy state.[12]

The diffusivity and diffusivity selectivity are functions of polymer properties on a molecular scale such as resistance to torsional motions, intersegmental backbone spacing, and free volume. Reductions in the mean interchain distance require larger segmental motions of polymer molecules to allow local passage of a gas molecule.

**2.2. Transport in Heterogeneous Materials.** Numerous models have been developed to describe transport properties in heterogeneous polymer systems. One of the most known ones is that of Maxwell[10,13,14] used in two forms. The simple form analyzes the steady-state dielectric properties of a dilute suspension of spheres where the permeability of a composite, $P$, made by dispersing of nonporous, impermeable filler (as $C_{60}$) in a continuous polymer matrix is expressed as

$$P = P_p\left(\frac{1 - \phi_f}{1 + \frac{\phi_f}{2}}\right) \quad (4)$$

where $P_p$ is the permeability of the pure polymer and $\phi_f$ is the volume fraction of filler. Equation 4 suggests that the permeability of the filled polymer is lower than of the pure polymer and decreases with increasing of the filler concentration. The decreased permeability is the result of a reduction in penetrant solubility due to (i) the replacement of polymer through which transport may occur with filler particles and (ii) an increase in the tortuosity[10] of the diffusion path through which the penetrant molecules cross the polymeric film. It is important to note that in the case of clustering of filler particles, and the formation of interstitial voids with no polymer into them, the structure gets more complex by inducing morphological changes in the polymer matrix.

The second generalized form[14] is used to estimate the permeation through a structured biphasic material wherein the additive component is randomly dispersed with sharp interfaces in a continuous matrix of the polymer expressed as

$$P = P_p\left[1 + \frac{(1 + G)\phi_f}{\left(\frac{P_f/P_p + G}{P_f/P_p - 1}\right) - \phi_f}\right] \quad (5)$$

where $P_f$ is the permeability of the $C_{60}$ and $G$ is a geometric factor accounting for dispersion shape. If the dispersed phase is oriented in lamellae parallel to the direction of permeation, $G \rightarrow \infty$, and there is minimum resistance to flow. If the disperse phase is oriented in lamellae perpendicular to the direction of permeation, $G \rightarrow 0$, and maximum impedance of flow occurs due to obstructive layers of the less permeable component. In this work, the $C_{60}$ volume fraction in PPO has been estimated using the equation

$$\phi_f = \frac{w_f}{w_f + \frac{\rho_f}{\rho_p}(1 - w_f)} \quad (6)$$

where $\rho_p$ and $\rho_f$ are the density of the pure polymer and $C_{60}$, respectively, and $w_f$ is the $C_{60}$ weight fraction in the polymer.

## 3. Experimental Section

**3.1. Modification of PPO.** The preparation of PPO−$C_{60}$ bonded polymer was performed in three steps:[3] (a) PPO bromination (PPO−Br), (b) PPO−Br conversion into PPO−$N_3$, and (c) PPO−$N_3$ conversion into PPO−$C_{60}$ bonded. The bromination of PPO is a selective reaction that can introduce bromine into the phenylene rings or into the benzyl position.[15−17] In our work, free radical bromination of PPO was carried out to provide PPO containing bromomethyl groups, and it was subsequently used for the preparation of PPO−$N_3$[17]. The bromomethylation of PPO was confirmed by $^1$H NMR spectroscopy (using a Varian Unity INOVA 300 MHz spectrometer).

**3.2. Preparation of Membranes.** Membranes of PPO pure, PPO−$C_{60}$ bonded, and dispersed at various concentrations (0.5 − 2.0 wt %) were prepared using the method described elsewhere.[3] There is a limit in the preparation of PPO−$C_{60}$ bonded membrane. Above 2.0 wt % $C_{60}$, the polymer becomes insoluble, intractable, and not processable. In contrary, for PPO−$C_{60}$ dispersed membrane there is no such limit regarding the $C_{60}$ concentration. Besides, $C_{60}$ undergoes aggregation in polar aromatic solvents like benzonitrile (BZN) and benzyl alcohol (BZA) but not in relatively nonpolar solvents like benzene (BZ), toluene (TL), and chlorobenzene (CBZ).[18] Therefore, to avoid the $C_{60}$ aggregation, we have used chlorobenzene as a solvent for the preparation of the PPO−$C_{60}$ membranes. Since the membrane structure depends on the casting solvent,[19] PPO pure membranes were prepared in chlorobenzene and chloroform for comparison. The thickness of all membranes was in the range 50−100 $\mu$m. After the preparation, the samples were mainly stored in vacuum oven at 30 °C. Some samples have also been stored at 100 °C to study the membrane aging.

**3.3. Characterization of Membranes.** The thermal properties of pure PPO, PPO−$C_{60}$ bonded, and dispersed were measured using a Perkin-Elmer DSC-7 (differential scanning calorimeter) in a nitrogen atmosphere. The samples were initially heated from 50 to 350 °C, cooled with liquid nitrogen, held for 5 min, and reheated two more times following the same steps, under a nitrogen atmosphere. The heating rate was 10 °C/min, and the cooling rate was 20 °C/min. The glass transition temperature, $T_g$, of the polymer was obtained from the third scan.

The permeation of pure nitrogen ($N_2$), oxygen ($O_2$), and carbon dioxide ($CO_2$) through the PPO and PPO−$C_{60}$ (dispersed and covalently bonded) was investigated, using the setup described elsewhere.[20] Pure gas permeability coefficients were calculated from the steady-state pressure increase in time in a calibrated volume at the permeate side by using the equation

$$\frac{P}{l} = \frac{V \cdot 273.15(P_{pt} - P_{p0})}{AT\frac{P_{ft} + P_{f0}}{2} 76t} \times 10^6 \quad (7)$$

where the ideal gas law is assumed to be valid, $P_{pt}$ and $P_{ft}$ [bar] are the pressure at the permeate and feed side at time $t$, $P_{p0}$ and $P_{f0}$ are the permeate and feed pressure at $t = 0$, $T$ [K] is the temperature, $V$ [cm$^3$] is the calibrated permeate volume, and $A$ [cm$^2$] is the membrane area. The gas permeance ($P/l$) is expressed in GPU, i.e., $10^{-6}$ cm$^3$ cm$^{-2}$ s$^{-1}$ cmHg$^{-1}$. Multiplying the gas permeance with the thickness of dense membranes, $l$ [$\mu$m], gives the permeability coefficient in barrers. All the gas permeation experiments were performed at 35 °C. Values and error bars reported in the tables and figures are based on measurements of two different membrane samples.

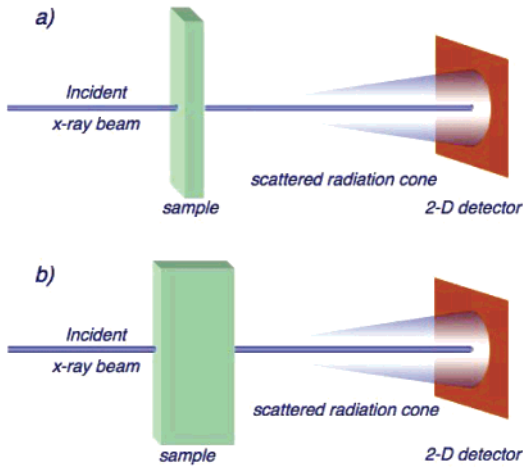


**Figure 1.** Sample geometry used in the WAXS experiments incident X-ray beam: (a) perpendicular to the film plane; (b) on the side of the film.

The gas sorption isotherms of $N_2$, $O_2$, and $CO_2$ in dense PPO pure and PPO−$C_{60}$ bonded and dispersed (1.5 wt %) films were measured at 35 °C, using a magnetic suspension balance[21] (MSB, Rubotherm). The experimental procedure was divided into five steps: (a) evacuation of pressure vessel and sample for at least 24 h; (b) increase of gas pressure to desired value; (c) wait until equilibrium in mass change is reached; (d) record equilibrium mass, temperature, and pressure; (e) repeat steps b and c or if the maximum pressure is reached: evacuate sample (step a) and start measurement with new gas or new sample. The equilibrium mass increase was corrected for buoyancy by subtracting the weight at zero sorption at a certain pressure from the vacuum weight of the sample. Using the equilibrium weight increase and the density of the polymer, the concentration (in $cm^3$ STP) inside the polymer ($cm^3$ polymer) was calculated.[21]

**3.4. WAXS Measurements.** Knowledge of crystalline morphology is of great importance in understanding the permeation properties of the polymeric membranes. In general, the crystalline phase may be regarded as impermeable. For this reason the gas permeability in a semicrystalline polymer membrane is substantially lower than in the more amorphous membrane because of the reduced space available for diffusion and the tortuous path around the crystallites. Permeation sites may be of either amorphous material or interstices between crystallites.[19]

The most generally applicable technique that provides information about the crystalline structure is the X-ray diffraction (XRD). In this study, wide-angle X-ray scattering (WAXS) experiments were performed using a Bruker-Nonius D8-Discover equipped with a 2-D detector. Standard background (air and sample holder) subtraction measured at the same time and conditions were applied to all data. The sample−detector (S−D) distance was set at 10 cm, and the incident beam wavelength was 1.54 Å (Cu Kα). Measurements were performed both perpendicular and in the plane of the membrane (see Figure 1). In the first case, the sample thickness as seen by the incident beam was always less than 0.5 mm.

## 4. Results and Discussion

**4.1. H NMR.** The $^1$H NMR chemical shift values (300 MHz) are reported as $\delta$ in [ppm] using the residual solvent signal as an internal standard ($CDCl_3$ $\delta$ = 7.29). $^1$H NMR spectra in $CDCl_3$ were performed for PPO pure and PPO−Br 2 wt %. The spectrum of the pure compound shows two singlets: one at 2.11 ppm for the methyl protons and one at 6.49 ppm for the aromatic protons. The spectrum of the 2% brominated compound shows, besides the two singlets, an extra peak at 4.36 ppm specific for the $CH_2Br$ protons.[15] This confirms that the bromination has taken place on the methyl group, and the further modification by coupling of $C_{60}$ took place on the methyl group of PPO, too.

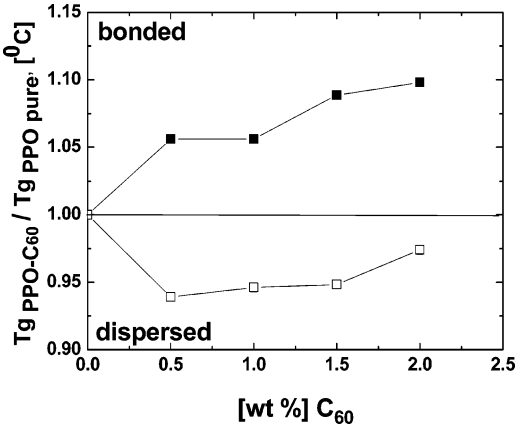


**Figure 2.** $T_g$ of PPO−$C_{60}$ bonded and dispersed over $T_g$ of pure PPO membranes vs the wt % $C_{60}$ content.

**4.2. DSC $T_g$.** Figure 2 shows that the $T_g$ of PPO−$C_{60}$ bonded increases with the increase of the $C_{60}$ concentration, from 214 °C for the pure PPO to 235 °C for the PPO−$C_{60}$ 2 wt %. This indicates that the PPO−$C_{60}$ bonded polymer becomes more stiffened, and probably there is suppressed interchain packing due to hindering the torsional motion of the phenyl ring around the ether linkage as well as some possible conformational changes in the backbone. Perhaps, as a consequence an extra interstitial chain space is created, and the free volume of the membrane increases, too. In contrast, for the PPO−$C_{60}$ dispersed membranes the $T_g$ decreases in comparison to pure PPO, indicating a more compact polymer structure in agreement with literature.[22] More detailed investigation of the PPO−$C_{60}$ structure (bonded and dispersed) using positron annihilation lifetime spectroscopy (PALS) and dielectric relaxation spectroscopy is currently under investigation and will be the subject of a future submission.

**4.3. WAXS Analysis.** It is well-known that the $C_{60}$ show anomalous behavior due to the formation of aggregates.[23,24] Figure 3 shows the results recorded in a 2-D detector for PPO−$C_{60}$ bonded and dispersed with 2.0 wt % $C_{60}$. The scattering from the pure $C_{60}$ powder and pure PPO is also shown for comparison. For PPO−$C_{60}$ the incident beam geometry corresponds to Figure 1a, the incident beam perpendicular to the film plane. The scattering pattern of $C_{60}$ powder (see Figure 3a) exhibits typical crystalline structure. The peak positions are displayed in Figure 5a as a function of the scattering angle and are indexed following the convention used in the literature.[25] The scattering of the pure PPO film is also displayed (Figure 5b), and it is in agreement with previously published data.[19] Some of the scattering peaks in $C_{60}$, namely (111) and (220), are used as references in the interpretation of the scattering from bonded and dispersed films. They correspond to *d*-spacings of 14.17 Å, the crystalline face-centered-cubic (fcc) lattice constant, and 7.53 Å, the $C_{60}$ diameter (Figure 5a).

The scattering peaks from $C_{60}$ (Figure 3a), as well as those of the pure PPO films (Figure 3b), are also present in the scattering patterns of the bonded and dispersed films (see parts c and d of Figure 3, respectively). Despite the fact that both samples contain the same amount of fullerene (2 wt %), the scattering fullerene peaks, (111) and (220), are far more intense in the PPO−$C_{60}$ dispersed. This intensity scattering difference in bonded and dispersed samples as a function of the scattering angle, $2\theta$, can be easily observed in Figure 5b,c.

We assume that the peak (*) comes from the PPO since it is present in all PPO−$C_{60}$ bonded and dispersed samples and in

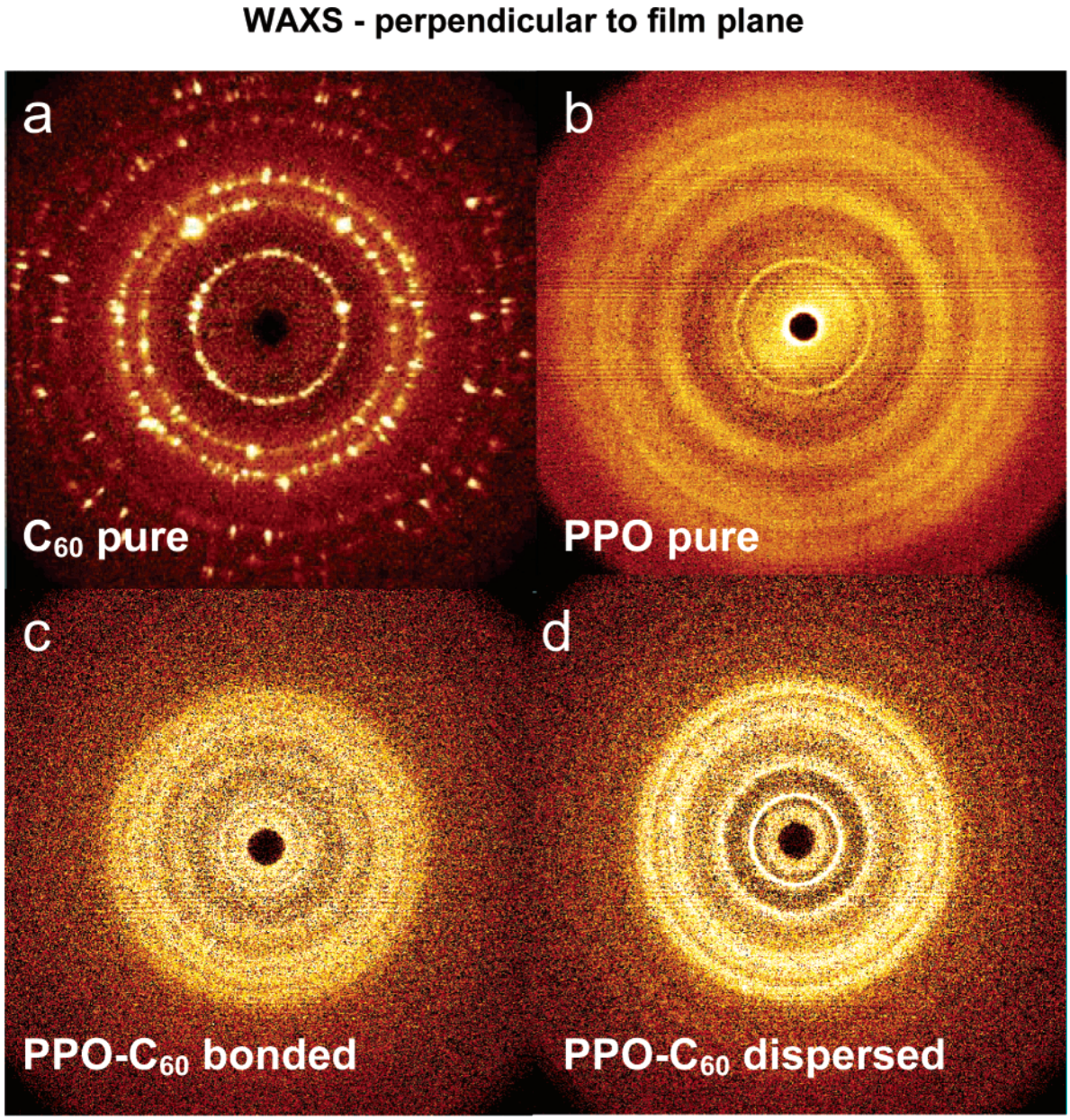


**Figure 3.** Scattering data recorded on a 2-D detector for the two basic components of the samples: (a) pure $C_{60}$ powder, (b) pure PPO, (c) PPO−$C_{60}$ 2.0 wt % bonded, and (d) PPO−$C_{60}$ 2.0 wt % dispersed.

the pure polymer (see Figure 5c,d) and absent in the pure $C_{60}$ (Figure 5a). The intensity changes in the (*) peak area of PPO−$C_{60}$ dispersed (Figure 5d) results from the influence of the presence of $C_{60}$ that may aggregate and simultaneously inducing more short-range order in the polymer. In the PPO−$C_{60}$ bonded, the (*) peak has low intensity, probably because the crystallization is less due to the hindrance of the rotational movements of the polymer segments by the presence of the $C_{60}$.

The peak around the (111) fullerene position seems much more distinct in the dispersed than in the bonded sample, strongly indicating clustering of fullerene in the dispersed system. Note, however, that the pure polymer also exhibits a peak about the same position (Figure 5b). This could contribute to the scattering in the dispersed case, especially if the degree of fullerene clustering is large enough to provide the polymer more freedom to crystallize than that in the bonded system. This picture is also supported by the scattering of the PPO−$C_{60}$ bonded film where no peak at that position is observed, indicating absence of strong fullerene clustering in the bonded film. It also suggests partial suppression of crystallinity in the film containing bonded fullerene.

More evidence for fullerene clustering in the dispersed sample can be found in Figure 5d, where the scattering from samples containing different amounts of fullerene are displayed. The peaks indicating clustering of fullerene increase strongly with fullerene concentration in the dispersed films (Figure 5d) while it practically does not change in the case of bonded films (Figure 5c). Comparing both sets of diffraction patterns, it seems that clustering is the major factor of difference. The variation of polymer scattering peaks is more prominent in the dispersed case.

Enhancement of gas permeability is known to be partially driven by the amount of interface between the polymer and the filler particles, fullerenes in the present case. In the case of the dispersed samples, clustering of fullerenes diminishes the amount of interface between the two species, and therefore, it should in principle decrease the membrane permeability. Clustering of fullerene may, however, also decrease the

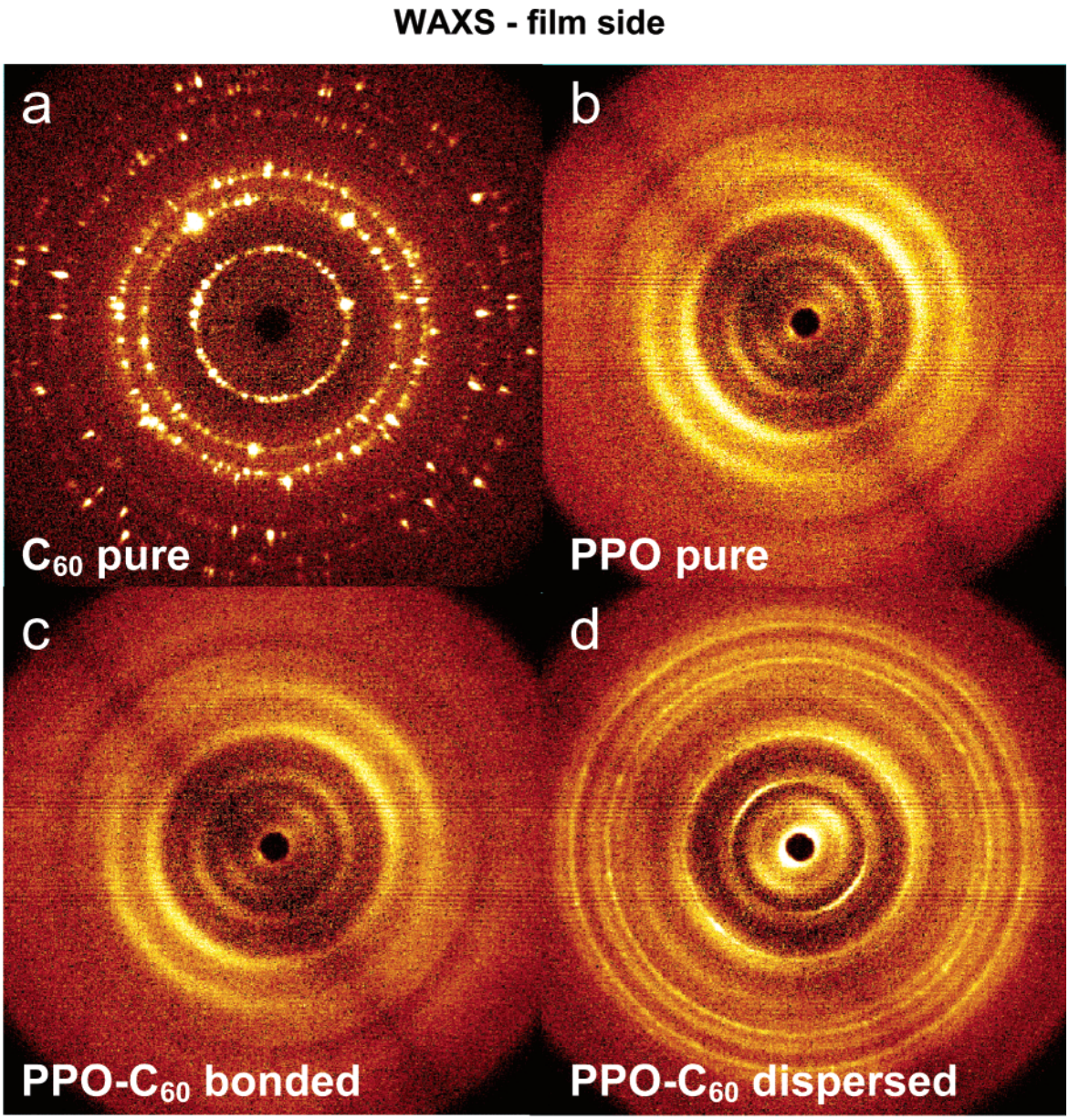


**Figure 4.** Scattering data recorded on a 2-D detector for the two basic components of the samples: (a) pure $C_{60}$ powder, (b) pure PPO, (c) PPO−$C_{60}$ 2.0 wt % bonded, and (d) PPO−$C_{60}$ 2.0 wt % dispersed.

membrane permeability by creating an extra barrier for gas transport. Not only the size and shape of the clusters are of importance but also their orientation in the sample may constitute the most important feature. Figure 4 shows the scattering of the two samples of bonded and dispersed films containing 2 wt % of fullerenes. In this case, the scattering geometry used is incident X-ray beam on the film side. Figure 4d clearly shows that the scattering peaks of the fullerenes in the dispersed case are very anisotropic. For instance, the (111) reflections corresponding to the fcc lattice distance of the fullerene clusters are croissant-shaped. They are also aligned along the film direction. Such a scattering clearly indicates that fcc unit cells are aligned along the film plane. A perfect alignment of an fcc monolayer would lead to a very bright delta-function scattering also aligned in the same direction. It is more reasonable to consider the observed scattering as the result of sheetlike fullerene aggregates that are aligned along the film plane. Variation of thickness and fluctuations on the alignment of such clusters certainly lead to such a croissant-like scattering patterns. Since the density of the fullerene molecules is far larger than that of the polymer, it is very probable that during the drying process segregation of the fullerenes occurs preferentially to the face of the film in contact with the glass plate. Figure 4c shows that this phenomenon is practically absent in the case of bonded samples, and if present, it concerns only a very small amount of the fullerene molecules that would search contact with the substrate.

In conclusion, the WAXS results indicate some significant changes in the polymer structure due to introduction of the fullerenes: For the PPO−$C_{60}$ bonded membranes; the crystallization is probably partially suppressed in comparison to PPO−$C_{60}$ dispersed. For the PPO−$C_{60}$ dispersed membranes, significant clustering of $C_{60}$ occurs. The clusters seem to align parallel to the film plane.

**4.4. Gas Permeability and Gas Sorption.** The gas permeability and selectivity of PPO prepared in the chloroform and chlorobenzene are the same within the experimental error of the gas permeability setup (see Appendix). Therefore, it is reasonable to conclude that these casting solvents have no significant influence on PPO structure. In this work, the

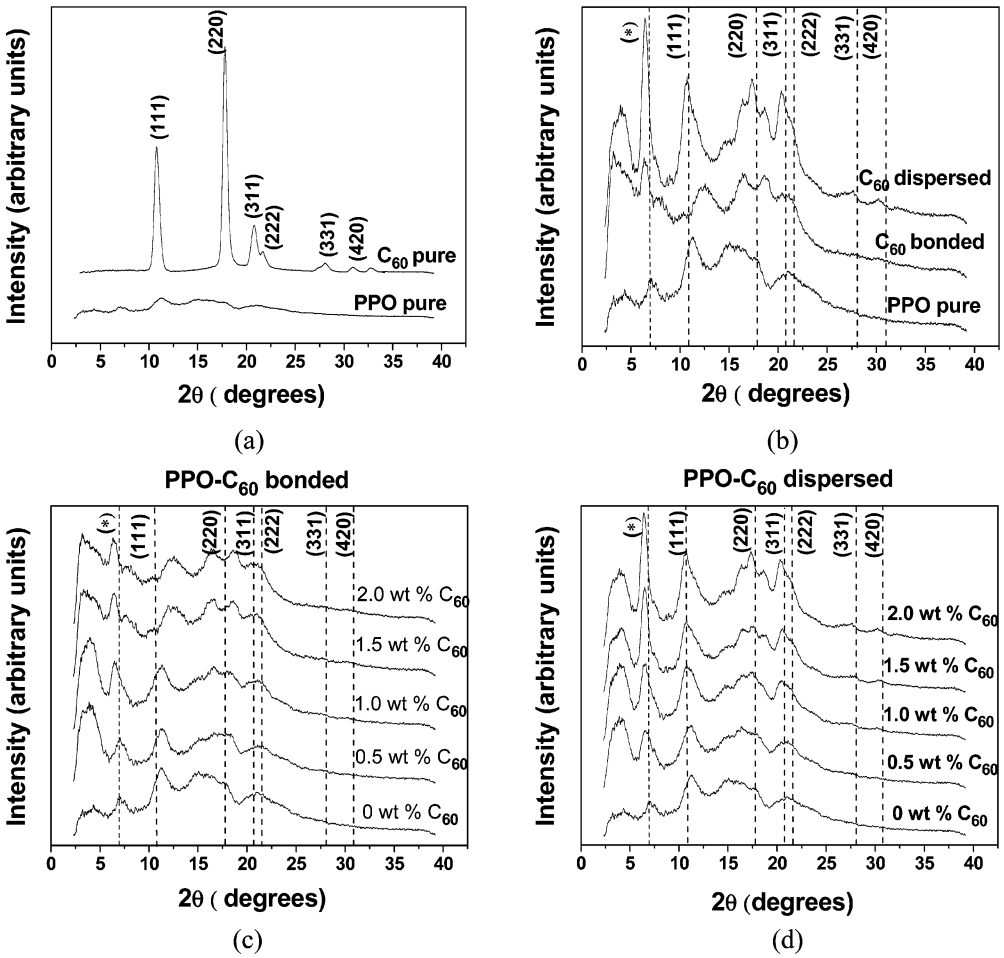


**Figure 5.** Scattering intensity as a function of the scattering angle: (a) Pure $C_{60}$ powder and pure PPO film cast with the same procedure as samples. (b) Pure PPO, PPO−$C_{60}$ 2 wt % bonded, and PPO−$C_{60}$ 2 wt % $C_{60}$ dispersed. The scattering peaks of pure $C_{60}$ are also represented (dashed lines). (c) Samples containing different amounts of bonded $C_{60}$. (d) Samples containing different amounts of dispersed $C_{60}$.

permeability of pure PPO prepared in chloroform will be compared with the permeability of PPO−$C_{60}$ bonded and dispersed.

The PPO−$C_{60}$ bonded and dispersed membranes were prepared using chlorobenzene solvent at various $C_{60}$ concentrations, 0.5, 1.0, 1.5, and 2.0 wt %. The color of the films becomes darker with the increase of $C_{60}$ content in both bonded and dispersed membranes. The type of interaction between the fullerene and PPO and also the influence of both components on structural and kinetic parameters of the PPO−$C_{60}$ system determine the physical properties of the polymer material. The PPO−$C_{60}$ bonded membranes are transparent, flexible, and mechanically stable. However, the PPO−$C_{60}$ dispersed membranes are not transparent and rather brittle. Their fragility increases with increasing of $C_{60}$ content.

Figure 6 and Table 1 show the comparison of the gas permeability of PPO−$C_{60}$ bonded and dispersed with the pure PPO membranes. The permeability coefficient significantly increases with the $C_{60}$ content for PPO−$C_{60}$ bonded. In contrast, it decreases for the PPO−$C_{60}$ dispersed. Besides, the gas permeability through pure PPO membranes and PPO−$C_{60}$ bonded and dispersed is constant at different feed pressure for all three gases measured $N_2$, $O_2$, and $CO_2$.[3] Table 2 presents the ideal gas selectivity at a feed pressure of 1.5 bar corresponding to the average of two different membrane samples. The average value might differ but if one takes in to account the standard deviation statistically they do not differ.

The DSC and WAXS results give an insight into the thermal and morphological parameters. In the PPO−$C_{60}$ bonded systems,

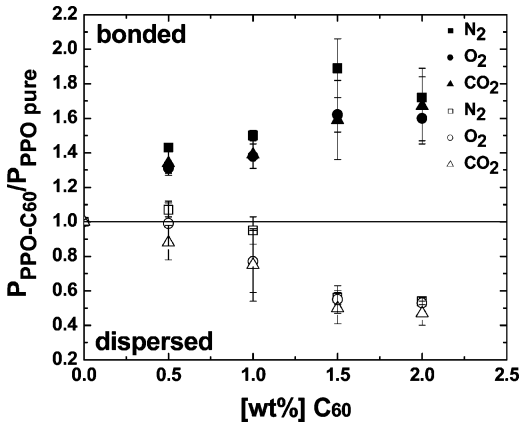


**Figure 6.** Permeability of PPO−$C_{60}$ normalized with the permeability of pure PPO vs the wt % $C_{60}$ content bonded for gases $N_2$ (■), $O_2$ (●), and $CO_2$ (▲) and for dispersed $N_2$ (□), $O_2$ (○), and $CO_2$ (△), at 1.5 bar feed pressure and 35 °C.

the stiffness of the chain probably increases (see $T_g$, in Figure 2) and the forced increase of interface between polymer and carbon cage enhances the free volume and the mobility of gas molecules at molecular scales and, therefore, permeability increases.

In the PPO−$C_{60}$ dispersed systems, the clustering of fullerenes (see WAXS results) probably decreases the interface between polymer and fillers, resulting in a decrease in free volume and mobility of gas molecules. This same segregation mechanism probably forms lamellae-like clusters parallel to the film plane.

**Table 1. Gas Permeability, Solubility, and Apparent Diffusivity of PPO Films[a]**

| | $N_2$ | | | $O_2$ | | | $CO_2$ | | |
|---|---|---|---|---|---|---|---|---|---|
| membrane | *P* | *S* | *D* | *P* | *S* | *D* | *P* | *S* | *D* |
| PPO pure | 2.7 | 8.4 | 3.2 | 11.7 | 11.0 | 10.7 | 50.7 | 78.3 | 6.5 |
| PPO−$C_{60}$ bonded 1.5 wt % | 5.1 | 8.9 | 5.8 | 19.1 | 15.3 | 12.5 | 80.8 | 90.2 | 9.0 |
| PPO−$C_{60}$ dispersed 1.5 wt % | 1.5 | 10.3 | 1.5 | 6.5 | 12.8 | 5.1 | 25.5 | 79.9 | 3.2 |
| change % bonded | 89 | 5 | 80 | 63 | 39 | 17 | 59 | 15 | 38 |
| change % dispersed | −44 | 22 | −54 | −45 | 16 | −53 | −50 | 2 | −51 |

[a] Feed pressure: 1.5 bar, $T = 35$ °C. *P* (barrers), *S* ($10^{-3}$, $cm^3$ (STP)/$cm^3$cmHg, *D* ($10^{-8}$, $cm^2$/s).

**Table 2. Ideal Gas Selectivity of PPO Films[a]**

| | selectivity | | |
|---|---|---|---|
| wt % $C_{60}$ in PPO | $P_{O_2}/P_{N_2}$ | $P_{CO_2}/P_{N_2}$ | $P_{CO_2}/P_{O_2}$ |
| 0 | 4.3 ± 0.1 | 18.7 ± 1.1 | 4.3 ± 0.3 |
| wt % $C_{60}$ bonded | | | |
| 0.5 | 4.0 ± 0.1 | 17.6 ± 0.3 | 4.4 ± 0.1 |
| 1.0 | 4.0 ± 0.2 | 17.3 ± 0.5 | 4.3 ± 0.2 |
| 1.5 | 3.7 ± 0.5 | 15.8 ± 2.9 | 4.2 ± 0.6 |
| 2.0 | 4.0 ± 0.5 | 18.1 ± 2.7 | 4.5 ± 0.7 |
| wt % $C_{60}$ dispersed | | | |
| 0.5 | 4.0 ± 0.6 | 15.3 ± 1.4 | 3.8 ± 0.7 |
| 1.0 | 3.5 ± 1.0 | 14.6 ± 4.6 | 4.2 ± 1.9 |
| 1.5 | 4.2 ± 0.8 | 16.7 ± 3.2 | 3.9 ± 1.0 |
| 2.0 | 4.3 ± 0.1 | 16.2 ± 1.8 | 3.8 ± 0.4 |

[a] Feed pressure: 1.5 bar, $T = 35$ °C.

The combination of these two mechanisms and the more compact structure (indicated by the lowering of $T_g$) contribute to the decrease in gas permeability as a function of fullerene concentration. In addition, for the PPO−$C_{60}$ dispersed probably there is a much higher crystalline gas impermeable fraction (due to the clustering) than in pure PPO or PPO−$C_{60}$ bonded. This can also contribute to decrease of gas permeability.

For the PPO−$C_{60}$ dispersed membranes, the Maxwell model (see eqs 4 and 5) has been used for the simulation of the experimental results. For all gases ($N_2$, $O_2$, and $CO_2$), the simple Maxwell model (eq 4) cannot represent the decrease of the permeability. The experimental results are always much lower than the predictions (see Figure 7, dotted lines). The generalized Maxwell model (eq 5), however, gives much better predictions (see Figure 7, full lines). For all cases, the estimated *G* parameter is low ($G_{N_2} = 0.02$, $G_{O_2} = 0.02$, $G_{CO_2} = 0.01$). These results suggest that the structure of the PPO−$C_{60}$ dispersed membranes contains lamellae $C_{60}$ clusters oriented perpendicular to the direction of permeation, consistent with the WAXS results. The $C_{60}$ clusters impede the gas diffusion through the material, resulting in reduced gas permeability.

Figure 8 presents the sorption isotherms of $CO_2$, $N_2$, and $O_2$ through PPO pure and PPO−$C_{60}$ bonded and dispersed at 35 °C. The sorption isotherms are fitted by the dual mode sorption model (see eq 3), and the obtained parameters are shown in Table 3. For $N_2$ the difference in sorption between the polymers is not significant. However, for $CO_2$ and $O_2$ the sorption is higher for PPO−$C_{60}$ bonded probably due to a lower crystallinity (as indicated by WAXS) and to the increase of free volume (as indicated by WAXS and DSC).

The sorption isotherms are necessary to deconvolute the permeability into its solubility and diffusivity contributions. Table 1 reports the permeability, solubility, and apparent diffusivity coefficients of $N_2$, $O_2$, and $CO_2$ gases in PPO, PPO−

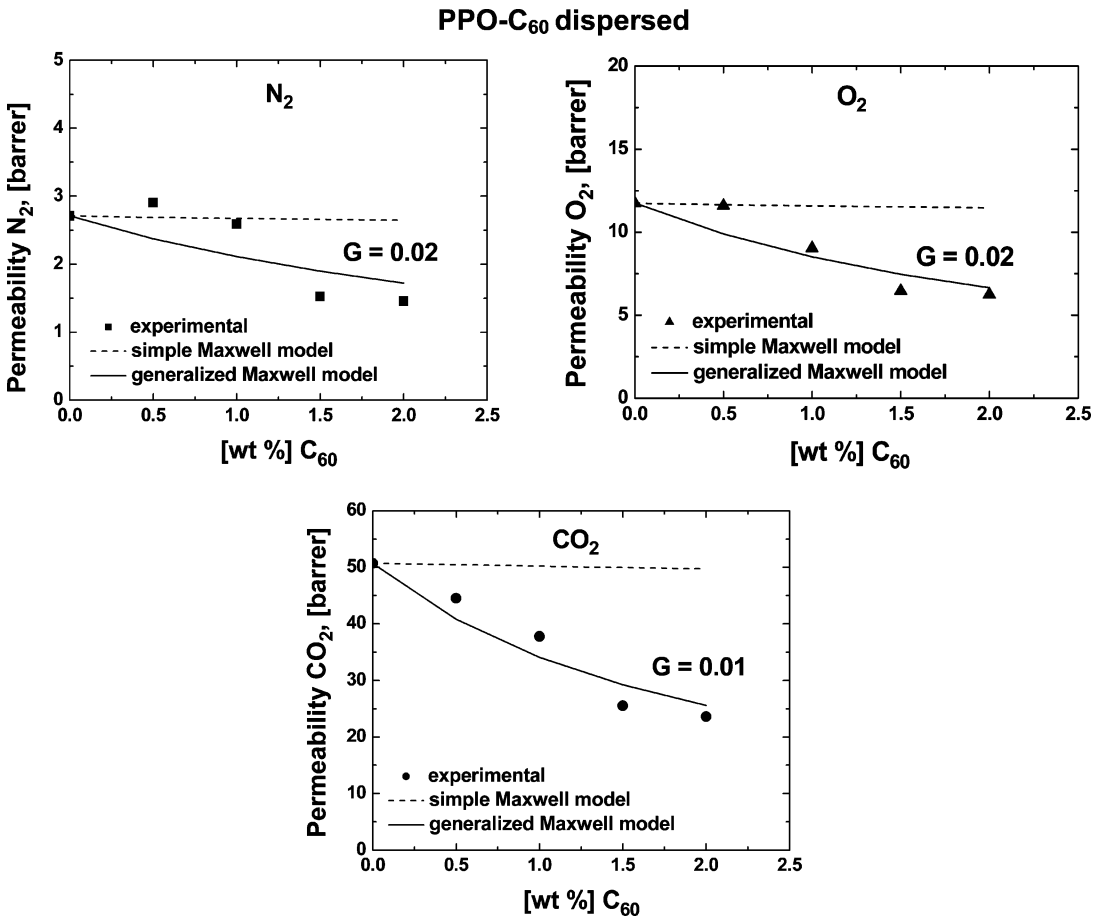


**Figure 7.** Gas permeability through PPO−$C_{60}$ dispersed vs the wt % $C_{60}$ content. The dotted line represents the prediction of simple Maxwell model. The solid line represents the prediction of generalized Maxwell model. The symbols represent the experimental results: (a) $N_2$ (■), (b) $O_2$ (▲), and (c) $CO_2$ (●).

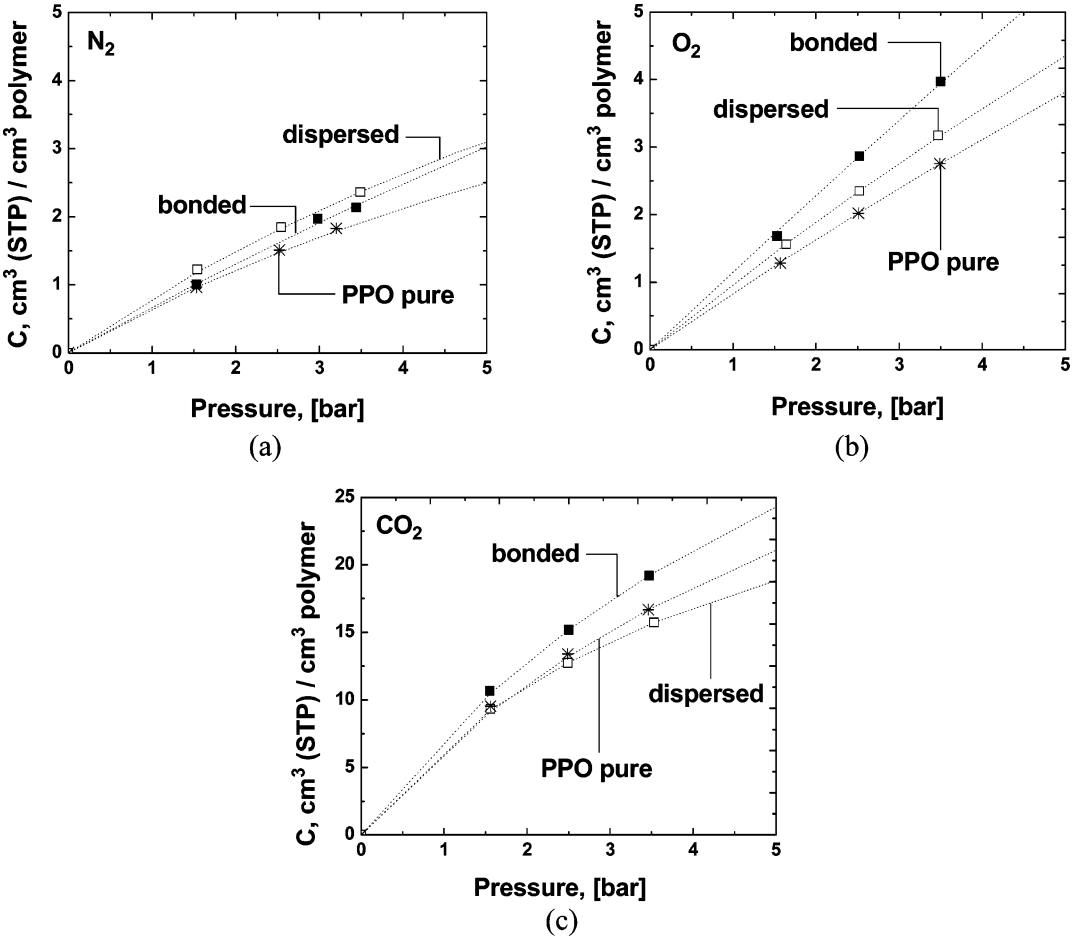


**Figure 8.** Sorption isotherms of (a) $N_2$, (b) $O_2$, and (c) $CO_2$ for of PPO−$C_{60}$ with 1.5 wt % $C_{60}$ content bonded (■) and dispersed (□) in comparison with pure PPO (*). The dotted lines are model lines, which are fitted according to the dual mode sorption model. $T = 35$ °C.

**Table 3. Dual Mode Sorption Parameters for $N_2$, $O_2$, and $CO_2$ in PPO Pure, PPO−$C_{60}$ Bonded, and Dispersed Films with 1.5 wt % $C_{60}$[a]**

| | $N_2$ | | | $O_2$ | | | $CO_2$ | | |
|---|---|---|---|---|---|---|---|---|---|
| membrane | $k_D$ | $C'_H$ | $b$ | $k_D$ | $C'_H$ | $b$ | $k_D$ | $C'_H$ | $b$ |
| PPO pure | 0.13 | 5.13 | 0.116 | 0.28 | 18.5 | 0.03 | 0.59 | 41.19 | 0.159 |
| PPO−$C_{60}$ bonded 1.5 wt % | 0.19 | 14.6 | 0.033 | 0.78 | 11.78 | 0.032 | 0.78 | 45.29 | 0.165 |
| PPO−$C_{60}$ dispersed 1.5 wt % | 0.27 | 4.12 | 0.158 | 0.45 | 11.4 | 0.047 | 0.67 | 26.4 | 0.29 |

[a] $k_D$ is expressed in $cm^3$ (STP)/($cm^3$ bar), $C'_H$ is expressed in $cm^3$ (STP)/$cm^3$, and $b$ is expressed in $bar^{-1}$. Pressure = 1.5/2.5/3.5 bar, $T = 35$ °C.

$C_{60}$ 1.5 wt % bonded, and dispersed, at 35 °C and 1.5 bar feed pressure. The solubility coefficient $S$ was estimated from the gas sorption measurements, and the apparent diffusion coefficient $D$ was calculated from the $P/S$ ratio.

The $N_2$ solubility coefficients are about equal for PPO−$C_{60}$ and PPO pure membranes. Then, the increase of $N_2$ permeability for the bonded membranes should be mostly attributed to increase of $D$. For $O_2$ and $CO_2$, however, the increase of permeability through the PPO−$C_{60}$ bonded in comparison to PPO pure membranes could be attributed to both increase of $S$ and $D$. Interestingly, the increase of $O_2$ permeability seems to be mostly due to increase of $S$ (39%) and of $CO_2$ mostly due to increase of $D$ (38%) (Table 1). For the PPO−$C_{60}$ dispersed, the decrease of gas permeability in comparison to PPO pure should be mostly attributed to decrease of $D$ (Table 1). This fits well with the results obtained with WAXS suggesting significant clustering and increase of crystallinity. Interestingly, the solubility of $N_2$ and $O_2$ to the PPO−$C_{60}$ dispersed membranes increases somewhat in comparison to pure PPO but of the $CO_2$ remains unchanged.

Finally, in order to get some insight into the aging of these membranes,[26,27] we stored samples in the vacuum oven at 30 and 100 °C for a year. Then, the gas permeability was measured again. The PPO−$C_{60}$ bonded membranes stored at 30 °C have the same high permeation properties as the freshly prepared ones. However, the membranes stored at 100 °C show 30−40% lower gas permeability than the fresh samples due to polymer aging.

## 5. Conclusions

The permeability of PPO−$C_{60}$ bonded increases with increasing of $C_{60}$ concentration. This is probably due to the stiffening of the polymer chain by the introduction of $C_{60}$ leading to increase of the polymer free volume.

The permeability of PPO−$C_{60}$ dispersed decreases with increasing of $C_{60}$ concentration. This is probably due to the clustering of the dispersed fullerene and the higher crystalline gas impermeable fraction (due to the clustering) than in pure PPO or PPO−$C_{60}$ bonded. The clusters seem to form lamellas oriented parallel to the membrane plane.

**Acknowledgment.** This work was financially supported by the Netherlands Organization for Scientific research (STW-NWO, project TPC.5776)

## Appendix

Pure PPO membranes were prepared using two different casting solvents: chloroform and chlorobenzene. Table 4 presents the gas permeability and selectivity of these membranes at 1.5 bar gas feed pressure and at 35 °C.

| casting solvent | permeability [barrers] | | | selectivity | | |
|---|---|---|---|---|---|---|
| | $N_2$ | $O_2$ | $CO_2$ | $P_{O_2}/P_{N_2}$ | $P_{CO_2}/P_{N_2}$ | $P_{CO_2}/P_{O_2}$ |
| chloroform | $2.7 \pm 0.1$ | $11.7 \pm 0.2$ | $50.7 \pm 2.6$ | $4.3 \pm 0.1$ | $18.7 \pm 1.1$ | $4.3 \pm 0.3$ |
| chloro-benzene | $3.3 \pm 0.3$ | $11.8 \pm 0.2$ | $47.0 \pm 7.2$ | $3.6 \pm 0.3$ | $14.2 \pm 3.2$ | $4.0 \pm 0.7$ |

## References and Notes

(1) Wang, Y.-C.; Huang, S.-H.; Hu, C.-C.; Li, C.-L.; Lee, K.-R.; Liaw, D.-J.; Lai, J.-Y. *J. Membr. Sci.* **2004**, *248*, 15.
(2) Freeman, B. D. *Macromolecules* **1999**, *32*, 375.
(3) Sterescu, D. M.; Bolhuis-Versteeg, L.; van der Vegt, N. F. A.; Stamatialis, D. F.; Wessling, M. *Macromol. Rapid Commun.* **2004**, *25*, 1674.
(4) Chen, Y.; Huang, Z. E.; Cai, R. F.; Yu, B. C. *Eur. Polym. J.* **1998**, *34*, 137.
(5) Dai, L. *Polym. Adv. Technol.* **1999,** *10*, 357.
(6) Geckler, K. E.; Samal, S. *Polym. Int.* **1999**, *48*, 743.
(7) Goh, S. H.; Zheng, J. W.; Lee, S. Y. *Polymer* **2000**, *41*, 8721.
(8) Albers, J. H. M.; Smid, J.; Kusters, A. P. M. US Patent 5.129.920, "Gas separation apparatus and also method for separating gases by means of such an apparatus", 1992.
(9) Mulder, M. *Basic Principles of Membrane Technology;* Kluwer Academic: London, 1992.
(10) Merkel, T. C.; Freeman, B. D.; Spontak, R. J.; He, Z.; Pinnau, I.; Meakin, P.; Hill, A. J. *Chem. Mater.* **2003**, *15*, 109.
(11) Kanehashi, S.; Nagai, K. *J. Membr. Sci.* **2005**, *253*, 117.
(12) Story, B. J.; Koros, W. J. *J. Polym. Sci., Part B: Polym. Phys.* **1989**, *27*, 1927.
(13) Merkel, T. C.; Freeman, B. D.; Spontak, R. J.; He, Z.; Pinnau, I.; Meakin, P.; Hill, A. J. *Science* **2002**, *296*, 519.
(14) Arnold, M. E.; Nagai, K.; Freeman, B. D.; Spontak, R. J.; Betts, D. E.; DeSimone, J. M.; Pinnau, I. *Macromolecules* **2001**, *34*, 5611.
(15) Cabasso, I.; Grodzinski, J. J.; Vofsi, D. *J. Appl. Polym. Sci.* **1974**, *18*, 1969.
(16) Verdet, L.; Stille, J. K. *Organometallics* **1982**, *1*, 380.
(17) Percec, V.; Auman, B. C. *Makromol. Chem.* **1984**, *185*, 2319.
(18) Nath, S.; Pal, H.; Sapre, A. V. *Chem. Phys. Lett.* **2002**, *360*, 422.
(19) Khulbe, K. C.; Matsuura, T.; Lamarche, G.; Lamarche, A.-M. *J. Membr. Sci.* **2000**, *170*, 81.
(20) Barsema, J. N.; Kapantaidakis, G. C.; van der Vegt, N. F. A.; Koops, G. H.; Wessling, M. *J. Membr. Sci.* **2003**, *216*, 195.
(21) Visser, T.; Koops, G. H.; Wessling, M. *J. Membr. Sci.* **2005**, *252*, 265.
(22) Polotskaya, G. A.; Gladchenko, S. V.; Pen'kova, A. V.; Kuznetsov, V. M.; Toikka, A. M. *Russ. J. Appl. Chem.* **2005**, *78*, 1468.
(23) Polotskaya, G. A.; Gladchenko, S. V.; Zgonnik, V. N. *J. Appl. Polym. Sci.* **2002**, *85*, 2946.
(24) Higuchi, A.; Agatsuma, T.; Uemiya, S.; Kojima, T.; Mizoguchi, K.; Pinnau, I.; Nagai, K.; Freeman, B. D. *J. Appl. Polym. Sci.* **2000,** *77*, 529.
(25) Weng, D.; Lee, H. K.; Levon, K.; Mao, J.; Scrivens, W. A.; Stephens, E. B.; Tour, J. M. *Eur. Polym. J.* **1999**, *35*, 867.
(26) Khulbe, K. C.; Matsuura, T. *J. Membr. Sci.* **2000**, *171*, 273.
(27) Nagai, K.; Nakagawa, T. *J. Membr. Sci.* **1995**, *105*, 261.

MA061300P